

## SUPPLEMENTARY INFORMATION

## High-amplitude fluctuations and alternative dynamical states of midges in Lake Myvatn

Anthony R. Ives<sup>1</sup>, Árni Einarsson<sup>2</sup>, Vincent A. A. Jansen<sup>3</sup>, and Arnþor Gardarsson<sup>2</sup>

<sup>1</sup>*Department of Zoology, UW-Madison, Madison, WI, 53706, U.S.A., email arrives@wisc.edu*

<sup>2</sup>*Myvatn Research Station and Institute of Biology, University of Iceland, Sturlugata 7, IS-101 Reykjavik, Iceland*

<sup>3</sup>*School of Biological Sciences, Royal Holloway, University of London, Egham, Surrey, TW20 0EX, U.K.*

### Supplementary Figures (pp. 1-11, Figs. S1-S9)

The Supplementary Figures give a mathematical investigation of the deterministic and stochastic properties of the midge-algae-detritus model.

### Supplementary Methods (pp. 12-15, Table S1, Fig. S10)

The Supplementary Methods describe the procedures we used to fit the models to data, and a brief analysis of data from another lake, Vikingavatn, Iceland.

### Supplementary Figures

Here we investigate the deterministic and stochastic properties of the midge-algae-detritus model given by equations 1-3. We initially address the general structure of the model and the genesis of the alternative dynamical states consisting of a stable point and a stable cycle. We then compare deterministic and stochastic properties of the model for the case in which parameter values give alternative dynamical states, and we follow this with a discussion of the case in which parameter values lead to only a stable point. Finally, we demonstrate that the stochastic dynamics are qualitatively indistinguishable between cases in which (a) alternative states exist, consisting of a stable point and a high-amplitude stable cycle, (b) only the stable point exists, and (c) only the high-amplitude cycle exists.

**Genesis of alternative states** – We investigated the structure of the deterministic model using continuity “bifurcation analyses” performed numerically, although we illustrate the results with simulations. The analyses showed that the alternative dynamical states, a stable point and a stable cycle, have different structural origins. We first detail the genesis of the locally stable point by documenting how it degenerates as the parameter  $q$  decreases from 1, with the other parameter values estimated from the Myvatn midge data. The locally stable point (Fig. S1a) first undergoes a supercritical Neimark-Sacker bifurcation (the discrete-time model equivalent of a supercritical Hopf bifurcation) near  $q = 0.739$ ; the fixed point loses stability and trajectories start to cycle away from the fixed point to converge towards a closed invariant set on which the dynamics show periodic or quasi-periodic behaviour (Fig. S1b). The closed invariant set exists

until  $q$  drops to 0.7366566 (Fig. S1c). At this point, the closed invariant set meets an unstable cycle of period 5 and disappears in a homoclinic bifurcation<sup>1</sup>. This homoclinic bifurcation is comparable to the textbook case of a homoclinic bifurcation between a invariant closed set and a saddle point (ref 1, p. 183) if one considers the period 5 iterated map (since the unstable period 5 cycle consists of 5 saddle points); as the bifurcation occurs, the invariant closed set meets the 5 fixed saddle points simultaneously. Once the stable invariant closed set has disappeared, all trajectories diverge from the fixed point (Fig. S1d) and converge to the large stable integer-period cycle associated with the population crashes described below (not shown in Fig. S1). Over much of the range of  $q$ , the unstable cycle of period 5 forms part of the boundary between the domains of attraction of the stable point or stable invariance closed set (formed by the supercritical Neimark-Sacker bifurcation of the fixed point) and the large integer-period stable cycle. The genesis of this unstable period 5 cycle appears to be a fold bifurcation (the discrete-time model equivalent of a saddle bifurcation) in which the unstable period 5 cycle appears coincident with a stable period 5 cycle, although we did not study this bifurcation in detail.

Outside the unstable period 5 cycle, there is a stable cycle whose origin is distinct from the bifurcations near the fixed point depicted in Fig. S1. Fig. S2 shows the domain of attraction to a small stable invariant closed set that exists when  $q = 0.738$ , with the boundary of this domain of attraction containing the unstable period 5 cycle. We plotted this domain as it intersects the plane that is tangent to the manifold containing the cyclic component of trajectories around the fixed point; this is the plane spanned by the complex eigenvectors of the Jacobian matrix at the fixed point, where the complex eigenvectors are portrayed in real canonical form<sup>2</sup>. Two trajectories (red) rapidly approach an outer cycle that has integer period.

The outer cycle is created by the lower boundaries of algae density  $y(t)$  and detritus density  $z(t)$  produced by small inputs given by the parameter  $c$ . The distinctive feature of this cycle is its strictly integer period. When midge densities  $x(t)$  are high, algae populations crash (towards the viewer in Fig. S2). Crashes in detritus and midges follow. Recovery occurs as the algae population grows exponentially, followed by detritus and midges, until the cycle repeats itself. The key feature generating the integer period is that the value of algae density after the population crash is reset to  $c$ , independent of the preceding densities of midges, algae, and detritus. This resetting of the algae population at  $c$  makes each successive population boom and bust relatively unaffected by the preceding boom and bust, causing trajectories to converge rapidly to an integer-period cycle.

**Stochastic dynamics with alternative states** – For the parameter values estimated from the data, there are two stable states. To investigate the stochastic dynamics, we relied on simulations to map the deterministic domains of attraction to the stable states, and then simulated stochastic dynamics on top of these maps to observe trajectories jumping between domains of attraction. Although the domains of attraction to the two stable states are 3-dimensional, topologically complex structures, we illustrate them by plotting the intersection between the domains of attraction and the plane that is tangent to the manifold containing the cyclic component of trajectories as they approach the stable point (Fig. S3a). In addition, we separate the domain of attraction to the stable point into regions in which trajectories approach the point with (light grey) or without (white) going through a population crash during which algae density hits the value  $c$ .

Figure S3a shows three trajectories, one (red line) initiating in the domain of attraction to the stable cycle (dark grey region), one (blue line) starting in that region (white) from which the

stable point is approached directly, and the last (green line) starting in that region (light grey) in which there is a single crash before the stable point is approached. The dots along each line give the points at which trajectories intersect the plane.

The domains of attraction to the stable point have different origins. The region of the domain in which trajectories move directly to the stable point (white) is derived from the analyses around the fixed point described in Fig. S1, with the boundary of the domain containing the unstable period 5 cycle. The region of the domain in which trajectories initially crash depends on the minimum algae density set by the input parameter  $c$ . As algae crash to the value  $c$ , the trajectory enters the domain of immediate attraction to the stable point (white region in Fig. S3b). In effect, the domain of attraction to the stable point captures populations as they hit the minimum algae boundary  $c$ . If there were no algae input ( $c = 0$ ), the population trajectories would pass through this plane to zero and would not be captured by the domain of attraction to the stable point.

In simulations of the stochastic case, there are clear transitions between the deterministic domains of attraction to the stable point and stable cycle (Fig. S4). The domain of attraction immediately around the stable point is relatively small, so that relatively small amounts of environmental stochasticity will cause a switch to the deterministic domain of attraction to the cycle. It should be noted that the transition between domains of attraction can occur outside the plane depicted in the figure. Also, because the domains of attraction are finely interdigitated, stochastic events may easily cause the domain of attraction to the stable point to catch trajectories on their return from population crashes.

We also plotted the fitted estimates of midge, algae, and detritus densities onto the depiction of the alternative states (Fig. S5). Of the 50 points in the time series, 24 are in the domain of attraction to the stable point, with 18 in the region giving direct approaches to the stable point and the remaining 6 in the region where trajectories initially crash. Thus, the domains of attraction to the stable point (24 points) and stable cycle (26 points) are roughly equally represented.

**Stochastic dynamics with only a stable point** – Throughout the space of parameters  $c$  and  $d$ , there are numerous regions in which only the stable point exists in the deterministic model (Fig. 3a). To illustrate the stochastic dynamics for these regions of  $c$ - $d$  parameter space, we used the parameter values fitted to the data but with  $c = 10^{-6.2}$  rather than the fitted value of  $c = 10^{-6.435}$  (Fig. S6). Although only the stable point exists for this value of  $c$ , its domain of attraction retains two qualitatively different regions: where the approach of trajectories to the stable point occurs without passing through a population crash (white region, with example trajectory in blue) vs. where a single population crash occurs (light grey region with green trajectory).

The region giving direct approaches to the stable point (Fig. S6) is essentially identical to the same domain when there are alternative states (Fig. S3). The loss of the stable cycle occurs because for this different value of  $c$  the trajectories experiencing population crashes enter the domain of attraction to the stable point at algae densities of  $c$ . Thus, the stable cycle is absorbed by the domain of attraction to the stable point.

Despite the absence of stable cycles, the stochastic dynamics are similar to the case with stable cycles (Fig. S7). With the addition of stochasticity, trajectories occasionally shift between the two regions giving either direct or indirect trajectories to the stable point. Because these two regions are finely interdigitated, relatively small amounts of stochasticity are required for these shifts.

**Qualitative similarity between cases with and without alternative states** – For the deterministic model, the cases with and without alternative dynamical states are qualitatively distinct. Nonetheless, in the stochastic model the qualitative dynamics are similar. Here, we demonstrate this for two comparisons. First, we compare the cases of a stable point with and without the existence of the high-amplitude integer-period cycle; this comparison is made by changing the value of  $c$  from  $10^{-6.435}$  to  $10^{-6.2}$  (Fig. 3a). Second, we compare the case with both stable point and stable cycle to the case in which there is a stable high-amplitude cycle but no stable fixed point; this comparison is made by changing the value of  $q$  from 0.903 to 0.70.

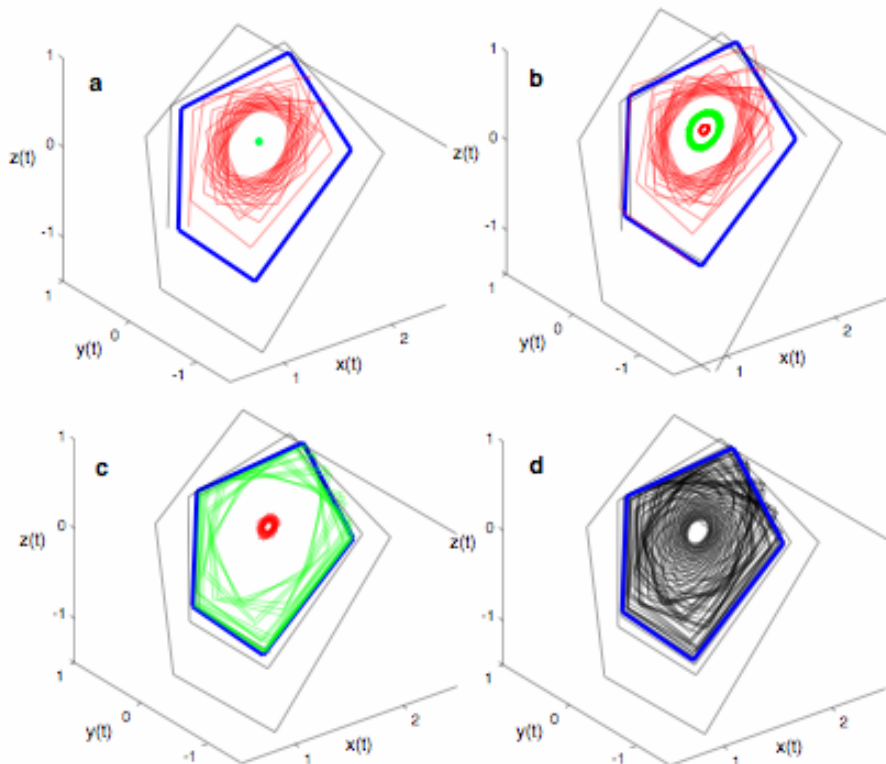
In the case with alternative states, irregular population crashes occur when there is a shift to the domain of attraction to the cycle. In the case with only a stable point ( $c = 10^{-6.2}$ ), the region of indirect trajectories that experience population crashes serves a similar dynamical role. Thus, time trajectories for the two cases look very similar (Fig. S8a,b). To illustrate the similarity of the stochastic dynamics for both cases, we computed the time interval (generations) between population crashes. This gives a relative measure of the frequency of shifts between domains of attraction when there are alternative states, or between regions of direct vs. indirect trajectories when there is only the stable point. The frequency distributions of time intervals between crashes are very similar for both cases (Fig. S9a,b). This illustrates how the stochastic dynamics for the case with only a stable point nonetheless pick up the ghost of the high-amplitude cycle as transients, and these transients are continuously exposed by stochastic fluctuations.

Fig. S8c depicts a time series when only the high-amplitude integer-period cycle exists in the deterministic skeleton ( $q = 0.70$ ); at this value of  $q$ , the fixed point is unstable (Fig. S1). Fig. S9c plots the frequency distribution of time intervals between crashes, which looks similar to that produced when there are both stable point and stable, high-amplitude cycle (Fig. S9a).

These cases illustrate that even when the deterministic skeleton does not show alternative states, the stochastic model shows dynamics reflecting the alternative states by picking up the transient behaviours of the deterministic skeleton. This is true for the case when only the stable point occurs in the deterministic skeleton (Fig. S9b) and when only the high-amplitude integer-period cycle occurs (Fig. S9c).

## References

1. Guckenheimer, J. and Holmes, P. Nonlinear oscillations, dynamical systems, and bifurcations of vector fields. (Springer-Verlag, New York, 1983).
2. Cronin, J. Differential equations: introduction and qualitative theory. (Pure and Applied Mathematics, volume 54). (Marcel Dekker, New York, USA, 1980).



**Fig. S1:** Genesis of a stable point surrounded by an unstable cycle in the midge-algae-detritus model (Eqs. 1-3). (a) Stable point surrounded by an unstable cycle when  $q = 0.7395$ . The stable point is shown in green, and the red trajectory eventually spirals to the stable point. The unstable period 5 cycle is shown in blue. The black trajectory is outside the unstable period 5 cycle and spirals outwards. (b) A supercritical Neimark-Sacker bifurcation occurs leading to a stable cycle when  $q = 0.7389$ . Three trajectories are depicted. Two trajectories are 10,000 points long, with the first 100 points shown in red and the last 100 points shown in green. Both of these trajectories are captured by the invariant closed set, which is given by the green circle. The third trajectory shown in black starts outside the domain of attraction to the invariant closed set and will eventually reach the stable high-amplitude integer period cycle (not shown). The unstable period 5 cycle is shown in blue. (c) Stable invariant closed set on the verge of a homoclinic bifurcation ( $q = 0.7366566$ ) in which it is eliminated by the unstable period 5 cycle (blue). One trajectory is 10,000 points long, with red and green lines showing the first and last 100 points of the trajectory. The end of the trajectory (green) is on the invariant closed set; the trajectory slows as it nears the unstable period 5 cycle. The second trajectory (black) is outside the unstable period 5 cycle and spirals outward towards the high-amplitude integer-period cycle (not shown). (d) Immediately following the homoclinic bifurcation ( $q = 0.73664$ ), the invariant closed set has been eliminated by the unstable period 5 cycle (blue), and trajectories move uniformly away from the fixed point. The ghost of the eliminated invariant closed set is still apparent as the trajectory slows near the unstable period 5 cycle before it passes through. Parameter values are those estimated from the data, with the exception of  $q$ :  $r_1 = 3.873$ ,  $r_2 = 11.746$ ,  $c = 10^{-6.435}$ ,  $d = 0.5517$ , and  $p = 0.06659$ . Values of  $x(t)$ ,  $y(t)$ , and  $z(t)$  are plotted on log scales. For convenience, the scaling term  $K$  is set to zero.

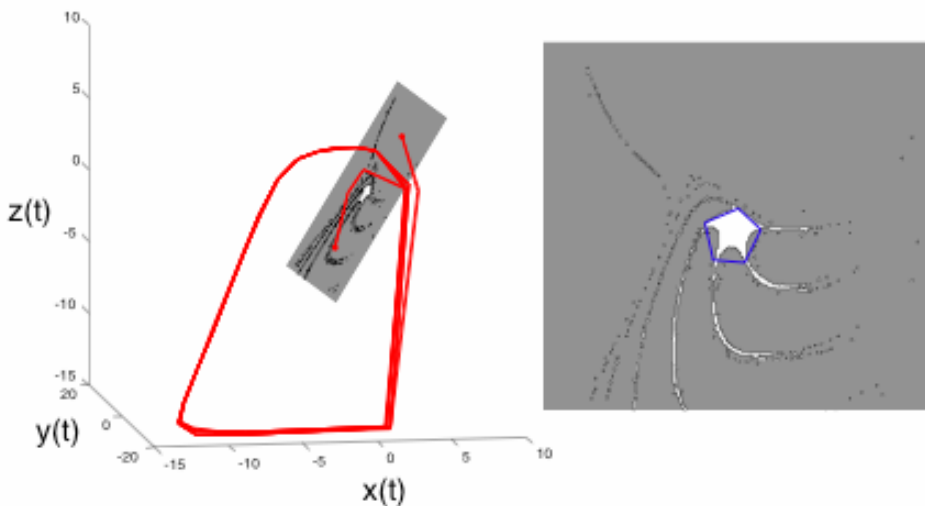


Fig. S2: Alternative stable states of the midge-algae-detritus model (Eqs. 1-3). The value of the parameter  $q = 0.738$  gives a small stable invariant closed set surrounded by an unstable cycle, and an outer stable cycle. In the panel on the left, the plane is tangent to the manifold containing the cyclic component of the dynamics around the stationary point; it is spanned by the vectors  $(v_1, v_2, v_3)$  and  $(u_1, u_2, 0)$ , where the two complex eigenvectors are  $(v_1 \pm u_1 i, v_2 \pm u_2 i, v_3)$ . The white region in the plane shows the domain of attraction to the invariant closed set, whereas the region in grey gives the domain of attraction to the outer stable cycle. The red lines give two examples of trajectories that converge to the outer stable cycle. The panel on the right shows the plane in more detail to illustrate the fine structure of the domain of attraction to the invariant closed set. The blue pentagon shows the unstable period 5 cycle that makes up part of the boundary between domains of attraction to the inner invariant closed set and outer stable cycle. Parameter values are those estimated from the data, with the exception of  $q$ ; see Fig. S1.

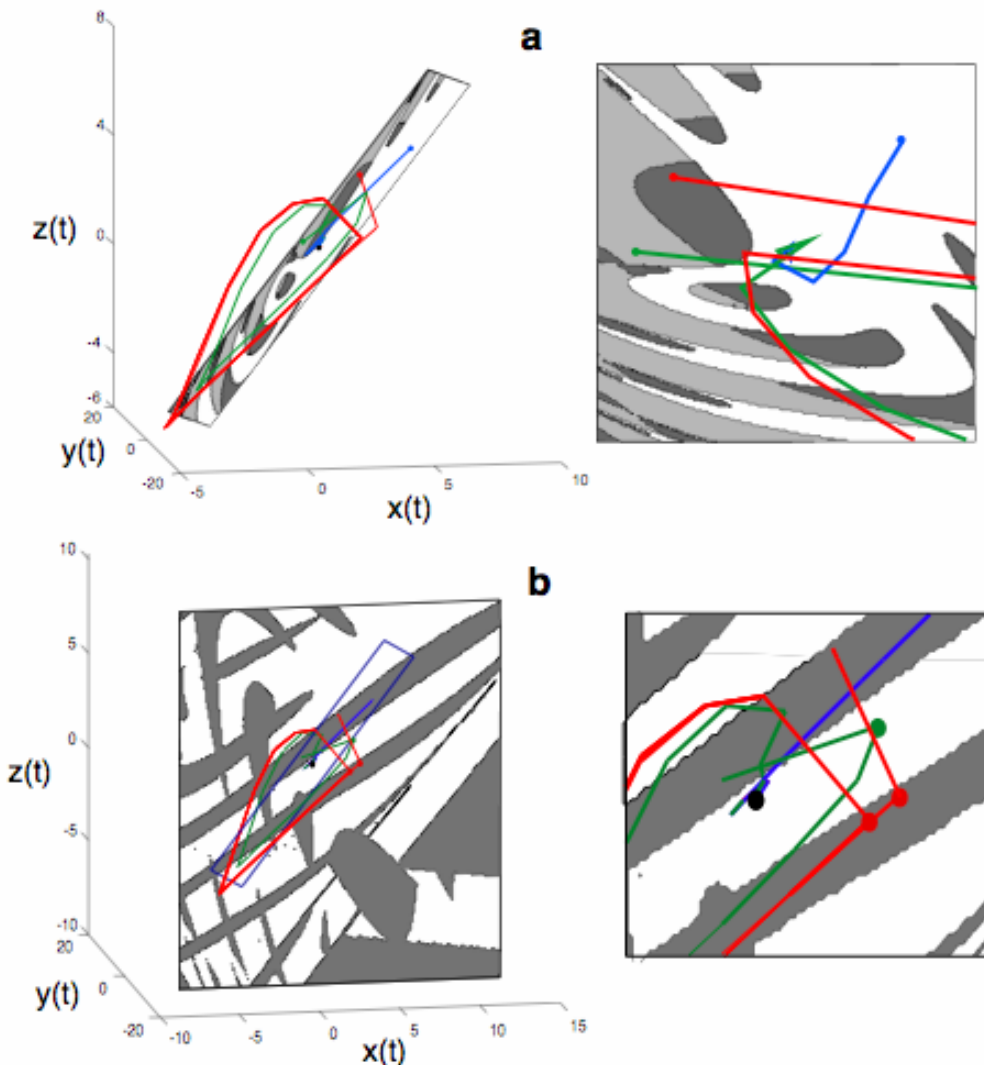


Fig. S3: Population dynamics of the midge-algae-detritus model (Eqs. 1-3) for parameter values estimated from the data that give alternative stable states. (a) The domains of attraction to the stable point and stable cycle are shown as they intersect the plane that is tangent to the manifold containing the cyclic component of the dynamics around the stable point. The domain of attraction to the stable cycle is shown in dark grey and is illustrated by the red trajectory. In the domain of attraction to the stable point, the white region has trajectories that travel directly to the stable point (blue trajectory), whereas the light grey region has trajectories that go through a population crash (green trajectory). Dots give intersections of the trajectories and the plane. (b) Like (a) but with the domains of attraction shown as they intersect with the plane on which  $y(t) = c$ . The plane from (a) is shown in outline. The panel on the right gives more detail of the points at which the trajectories intersect this plane (dots). Parameter values are:  $r_1 = 3.873$ ,  $r_2 = 11.746$ ,  $c = 10^{-6.435}$ ,  $d = 0.5517$ ,  $p = 0.06659$ , and  $q = 0.9026$ .

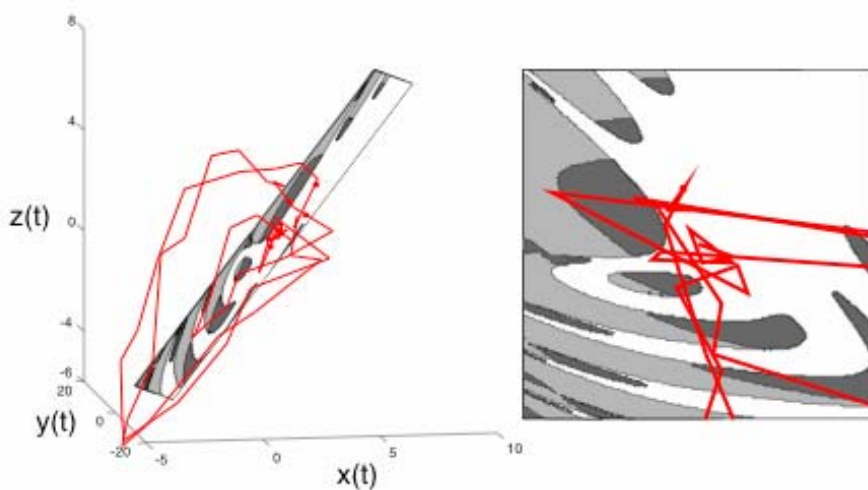


Fig. S4: Stochastic population dynamics of the midge-algae-detritus model (Eqs. 1-3) for parameter values estimated from the data and giving alternative states. A single 50-generation trajectory was simulated using the standard deviations of environmental stochasticity estimated from the data,  $\sigma_1 = 0.3491$  and  $\sigma_2 = \sigma_3 = 0.7499$ . See Fig. S3 for more details.

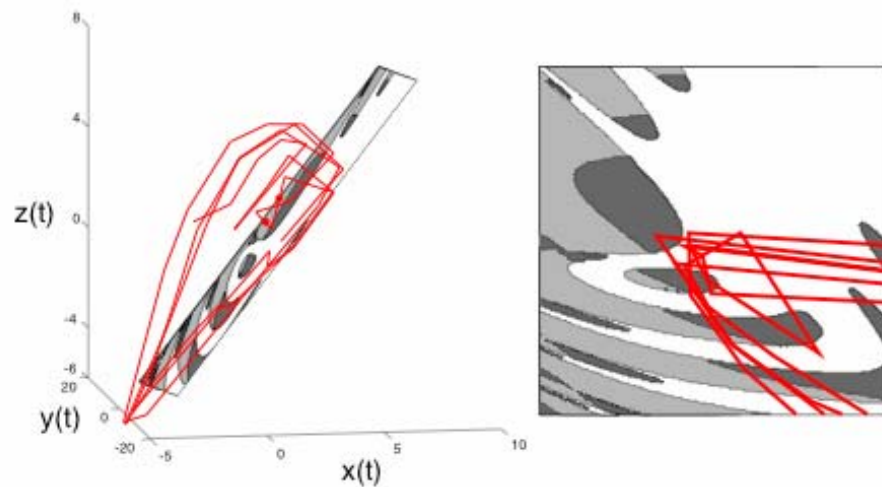


Fig. S5: Population dynamics of the midge-algae-detritus model (Eqs. 1-3) fitted to the observed data. The trajectory corresponds to the estimates of midge densities displayed in Fig. 1 (main text) obtained from the fitted model, with corresponding estimates of algae and detritus densities; see Supplementary Methods for fitting details. Domains of attraction to the alternative states were computed as in Fig. S4.

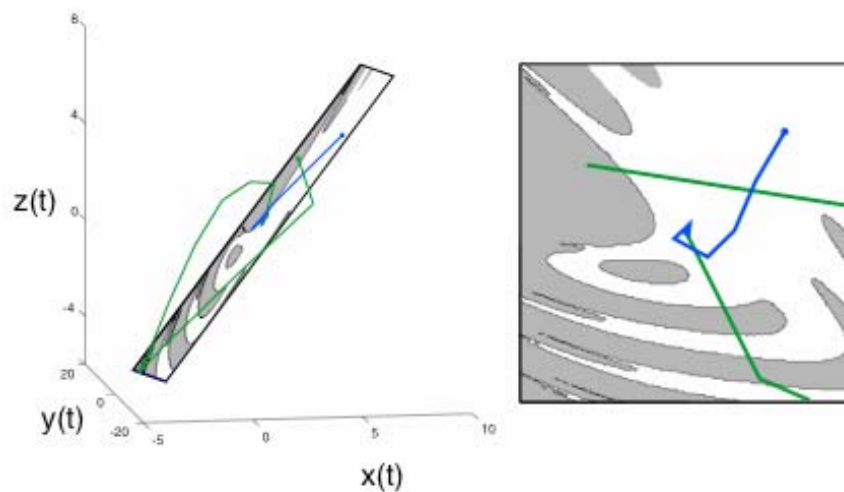


Fig. S6: Deterministic population dynamics of the midge-algae-detritus model (Eqs. 1-3) for parameter values giving only a stable point. The white region gives the domain in which trajectories approach the stable point directly (e.g., blue trajectory), whereas in the light grey region trajectories approach after a single crash (e.g., green trajectory). Parameter values are those estimated from the fitted data (Fig. S3) but with  $c = 10^{-6.2}$ .

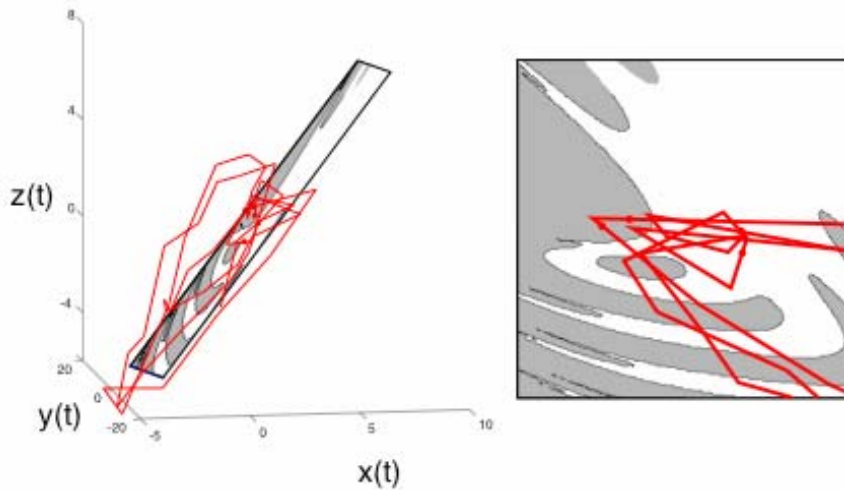


Fig. S7: Stochastic population dynamics of the midge-algae-detritus model (Eqs. 1-3) for parameter values giving only a stable point. A single 50-generation trajectory was simulated with environmental stochasticity estimated from the data,  $\sigma_1 = 0.3491$  and  $\sigma_2 = \sigma_3 = 0.7499$ . See Fig. S6 for details.

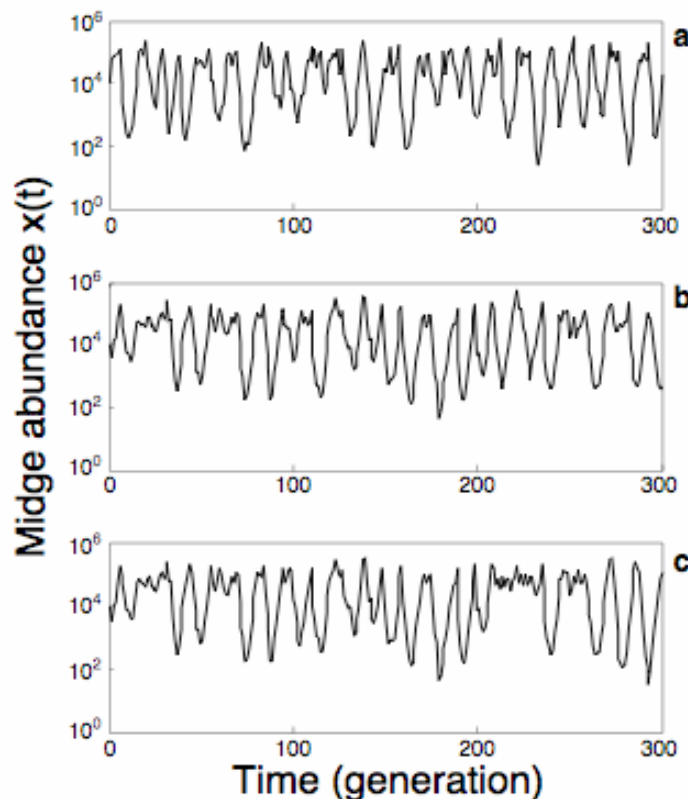


Fig. S8: Example 300-generation times series for the stochastic midge-algae-detritus model (Eqs. 1-3) with parameters giving either (a) alternative dynamical states, (b) only a stable point, or (c) only the high-amplitude integer-period cycle. Simulations were performed using the level of environmental stochasticity estimated from the data,  $\sigma_1 = 0.3491$  and  $\sigma_2 = \sigma_3 = 0.7499$ . Exactly the same sequence of environmental shocks (process errors) was used for all three panels to illustrate the differences caused solely by differences in model parameter values. For (a) the parameters are:  $r_1 = 3.873$ ,  $r_2 = 1.1746$ ,  $c = 10^{-6.435}$ ,  $d = 0.5517$ ,  $p = 0.06659$ , and  $q = 0.9026$ . For (b),  $c = 10^{-6.2}$ . For (c),  $q = 0.7$ .

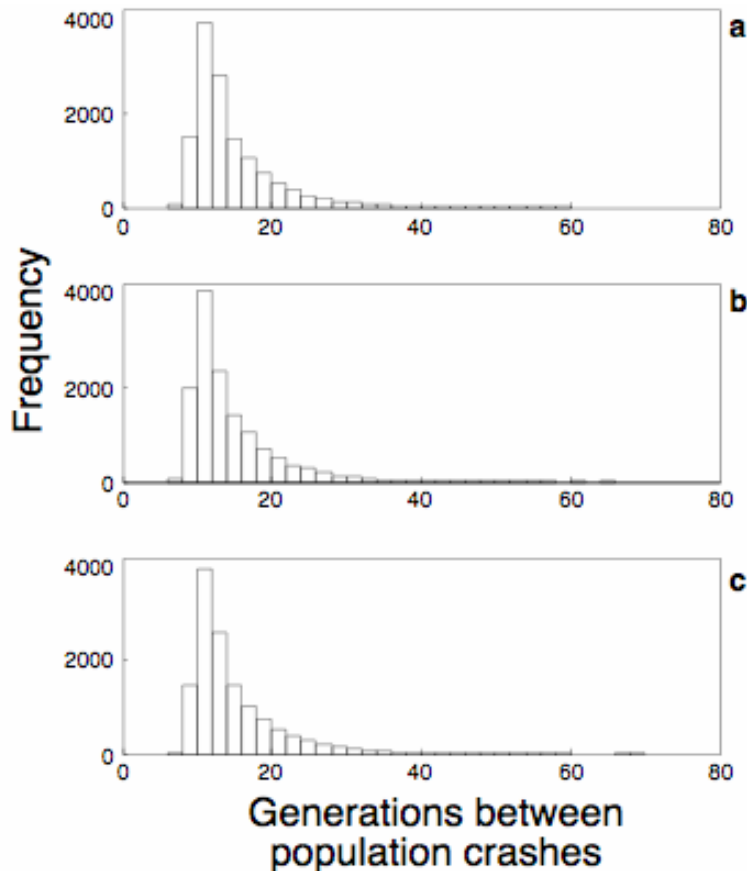


Fig. S9: Frequency of time intervals between population crashes produced by the stochastic midge-algae-detritus model (Eqs. 1-3) with parameters giving either (a) alternative dynamical states, (b) only a stable point, or (c) only the high-amplitude integer-period cycle. Simulations of  $2 \times 10^5$  generations were performed using the same parameter values as Fig. S8.

## Supplementary Methods

In the Supplementary Methods, we describe the procedures we used to fit the models to data, and we also present a brief analysis of data from another lake, Vikingavatn, Iceland.

**Model fitting** – We fit all three models with the same procedure using a state-space model<sup>1</sup> that incorporates measurement error:

$$\begin{aligned} \mathbf{U}(t+1) &= F[\mathbf{U}(t)] + \boldsymbol{\varepsilon}(t) \\ X(t+1) &= \boldsymbol{\Gamma}\mathbf{U}(t) + K + \boldsymbol{\eta}(t) \end{aligned} \quad (\text{S1})$$

where  $\mathbf{U}(t) = \log \begin{pmatrix} x(t) \\ y(t) \\ z(t) \end{pmatrix}$  is the vector of log midge, algae, and detritus abundances,  $F[]$  is the 3-dimensional function given by equations 1-3, 4, or 5 in the Technical Box,  $\boldsymbol{\varepsilon}(t) = \begin{pmatrix} \varepsilon_1(t) \\ \varepsilon_2(t) \\ \varepsilon_3(t) \end{pmatrix}$ ,  $X(t)$  is

the observed mean log midge abundance,  $\boldsymbol{\Gamma} = (1, 0, 0)$ ,  $K$  is a scaling term that sets the overall midge abundance, and  $\boldsymbol{\eta}(t)$  is a normal random variable with mean zero giving measurement error. The standard deviation of  $\boldsymbol{\eta}(t)$ ,  $\sigma_m$ , was estimated from the difference in midge abundances sampled from the two traps in a given generation. Specifically, given two replicate measurements of log midge density  $X_1$  and  $X_2$  each having standard deviation  $\sigma_m$ , the difference between the two measurements is  $X_1 - X_2$  has standard deviation  $\sqrt{2} \sigma_m$ . Therefore, we estimated the measurement error as  $1/\sqrt{2}$  times the standard deviation in the difference between replicate measures. Statistical diagnostics suggested that this estimate of  $\sigma_m$  was too large, so for fitting we reduced it by  $1/2$  which improved diagnostics. Reducing the measurement error during statistical fitting forces the models to fit the observed dynamics more closely and produces tighter predictions to the observed data.

Even though the dynamics of the models are given by three equations, only one of the variables, log midge abundance  $X(t)$ , was observed. Equation S1 was fit to these data using an extended Kalman filter<sup>1</sup> that gives the approximate likelihood function for the models given the data. Because the likelihood surface was not simply concave in the parameter values, we alternated between simulated annealing and simplex minimization to obtain the approximate maximum likelihood (ML) parameter estimates. Before model fitting, a small seasonal component of the data ( $\log_{10}$  spring abundances were consistently 0.53 higher than summer abundances) was removed by adding 0.53 to the summer abundances. Parameter estimates for the midge-algae-detritus model are given in Table S1.

To obtain statistical confidence in the existence of alternative dynamical states in the data, we fit the midge-algae-detritus model (Eqs. 1-3) constraining values of  $q$  to be sufficiently low that no stable point or internal, low-amplitude stable cycle existed; for the other parameter values estimated from the data, this occurs for  $q < 0.737$  (see Supplementary Figures). The threshold value of  $q$  below which a stable point or internal stable cycle disappear also depends on

the other parameters of the model. Therefore, when  $q$  was simply constrained to be less than 0.737, the estimates of other parameter values would produce a model having alternative dynamical states even though  $q < 0.737$ . Therefore, in fitting the model, we imposed constraints on other parameters to ensure that alternative dynamical states were not possible. Using the best-fitting parameter values not giving alternative dynamical states, we assessed the statistical significance of the difference between this and the unconstrained model using a likelihood ratio test.

**Goodness of fit** – To compare models, we used four measures of goodness of fit. The first is the  $-2 \log$  likelihood ( $-2\text{LL}$ ) computed from the extended Kalman filter. For the midge-algae-detritus and Lotka-Volterra models, the likelihood functions are approximations, although it is exact for the Gompertz log-linear model. Despite being approximations for nonlinear models,  $-2\text{LL}$  values give reasonable measures of goodness of fit. We also computed three types of  $R^2$  values. The Kalman filter uses a two-step procedure for estimating the log midge abundance in generation  $t + 1$ ,  $X(t+1)$ . First, it takes the estimated value of  $X(t)$ , denoted  $\hat{X}(t)$ , along with the associated estimates of algae and detritus abundances, to project the dynamics one generation forward using equations 1-3, thereby giving  $\hat{X}_p(t+1)$ . It then updates this predicted value by comparing it to the observed value  $X(t+1)$  and producing  $\hat{X}(t+1)$  that moves closer to  $X(t+1)$  to the extent dictated by the measurement error. Thus, there are two estimates of  $X(t+1)$ :  $\hat{X}_p(t+1)$  and  $\hat{X}(t+1)$ . Because  $\hat{X}_p(t+1)$  predicts  $X(t+1)$  using only information from generation  $t$ , the errors  $E(t+1) = X(t+1) - \hat{X}_p(t+1)$  include process errors  $\varepsilon_1(t)$ ,  $\varepsilon_2(t)$  and  $\varepsilon_3(t)$ , and measurement error  $\eta(t)$ . Because  $\hat{X}(t+1)$  predicts  $X(t+1)$  after factoring in measurement error, the errors  $\hat{E}(t+1) = \hat{X}(t+1) - \hat{X}_p(t+1)$  include only process error. The three  $R^2$  values are: (i) total  $R^2 = 1 - \text{var}E(t)/\text{var}X(t)$ , (ii) prediction  $R^2$  for  $\hat{X}(t+1) = 1 - \text{var} \hat{E}(t)/\text{var}[\hat{X}(t+1) - \hat{X}(t)]$ , and (iii) prediction  $R^2$  for  $X(t+1) = 1 - \text{var} E(t)/\text{var}[X(t+1) - X(t)]$ . Of these, the last is the standard measure of goodness-of-fit for state-space models<sup>1</sup>, although the second gives the best measure of goodness-of-fit when accounting for the effect of measurement error that unavoidably inflates the imprecision of the predictions.

**Fit to Vikingavatn Data** – To give additional evidence that the midge-algae-detritus model gives a reasonable fit to midge biology, we fit the model to data collected from Lake Vikingavatn using the same methods as the data collected in Myvatn (Fig. S10). The fit of the model to Vikingavatn is better than for Myvatn (Table S1), although this must be interpreted cautiously because of the small number of data points (18) available for Vikingavatn. In comparing parameter estimates, Vikingavatn had a higher resource input rate,  $c$ ; this can be explained by the smaller size of Vikingavatn ( $1.7 \text{ km}^2$  versus  $37 \text{ km}^2$  of Myvatn), making the benthos more open to inputs. The algae intrinsic rate of increase,  $r_2$  is much higher for Vikingavatn, although this parameter is poorly estimated due to the small sample size; the dynamics of the model are largely insensitive to values of  $r_2$  above 10.

## Reference

1. Harvey, A. C. *Forecasting, structural time series models and the Kalman filter*. (Cambridge University Press, Cambridge, U.K., 1989).

**Table S1:** Parameter estimates and measures of fit of the midge-algae-detritus model to Myvatn and Vikingavatn data

Parameter	Myvatn	Vikingavatn	Description
$r_1$	3.87	4.14	intrinsic rate of increase of midges
$r_2$	11.75	70.2	intrinsic rate of increase of algae
$\log_{10} c$	-6.435	-4.75	input rate of algae and detritus
$d$	0.552	0.820	retention rate of detritus
$q$	0.903	0.990	strength of density-dependent midge dynamics
$\log x(0)$	-1.943	2.45	initial midge abundance
$\log y(0)$	-0.369	1.46	initial algae abundance
$\log z(0)$	-0.0025	-6.5	initial detritus abundance
$K$	9.613	6.66	scaling factor for midge density
$p$	0.0666	0.0046	quality of detritus relative to algae
$\sigma_1$	0.349	0.004	variance of $\varepsilon_1(t)$ affecting midges
$\sigma_2 = \sigma_3$	0.750	0.093	variance of $\varepsilon_2(t)$ and $\varepsilon_3(t)$ affecting algae and detritus
$\sigma_m^{(1)}$	0.822	0.822	variance of measurement error
Data points	50	18	length of time series
-2LL	156.2	38.0	-2 * log likelihood function
Total R <sup>2</sup>	0.98	0.99	1 - varE(t)/varX(t) <sup>(2)</sup>
Prediction R <sup>2</sup> for $\hat{X}(t+1)$	0.74	0.91	1 - var $\hat{E}(t)$ /var[ $\hat{X}(t+1) - \hat{X}(t)$ ] <sup>(3)</sup>
Prediction R <sup>2</sup> for $X(t+1)$	0.53	0.83	1 - var $E(t)$ /var[ $X(t+1) - X(t)$ ]

<sup>(1)</sup> The measurement error variance was calculated independently using measurements from two traps at Myvatn.

<sup>(2)</sup>  $E(t) = X(t) - \hat{X}_p(t)$ , where  $\hat{X}_p(t)$  is the one-step-ahead prediction of log midge abundance made by equations 1-3.

<sup>(3)</sup>  $\hat{E}(t) = \hat{X}(t) - \hat{X}_p(t)$ , where  $\hat{X}(t)$  is the one-step-ahead prediction of log midge abundance after being updated by the observed value of  $X(t)$  to account for measurement error.

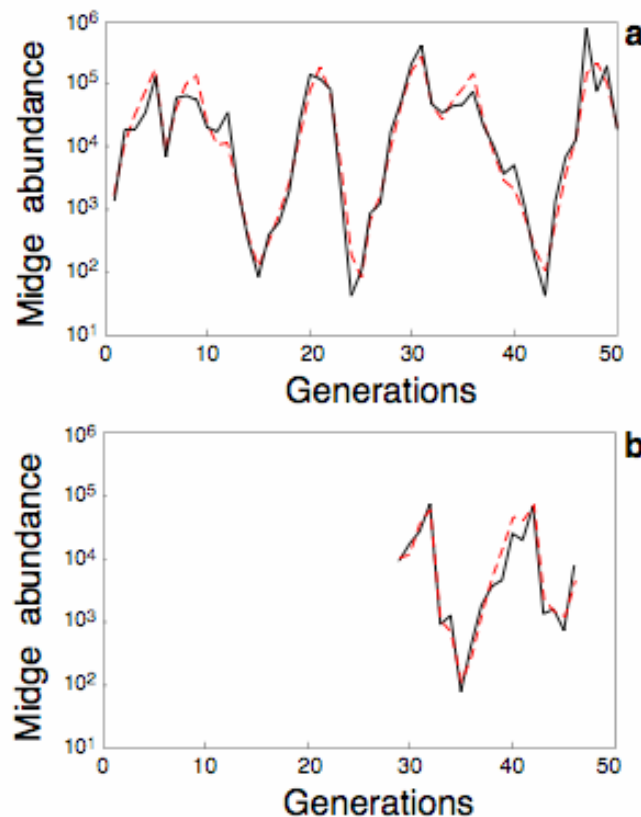


Fig. S10: Population dynamics of *T. gracilentus* in (a) Myvatn and (b) Vikingavatn. Black lines give the log abundance of midges per generation averaged between two traps in each lake. Red dashed line gives the predicted “true” (unobserved) abundances from the model given by equations 1-3 with parameter values estimated by maximum likelihood (Table S1).